Available online at www.sciencedirect.com
ScienceDirect
Journal of Power Sources 174 (2007) 624–627
JOURNAL OF POWER SOURCES
www.elsevier.com/locate/jpowsour

Short communication

Nano-tin alloys dispersed in oxides for lithium storage materials

Ying Zheng, Jun Yang *, Yanna NuLi, Jiulin Wang

Department of Chemical Engineering, Shanghai Jiao Tong University, Shanghai 200240, PR China

Available online 27 June 2007

Abstract

Finely dispersed tin alloy/oxide composites were synthesized via the reduction of tin oxide by aluminum under high-energy ball-milling. The morphology and crystal structure of the resulting samples were investigated by scanning electron microscopy (SEM), transmission electron microscopy (TEM), and X-ray diffraction (XRD). The electrochemical measurements reveal that Sn_3Co/Al_2O_3 composite has higher initial efficiency and better cycle performance than Sn/Al_2O_3. The Sn_3Co/Al_2O_3 composite electrode containing LA132 binder exhibited a reversible capacity about 540 mA h g^{-1} with good capacity retention. On the other hand, it is found that the influence of binder type on the electrode performance is remarkable.

Keywords: Tin–cobalt alloy; Oxide composite; Electrode binder; Li-ion batteries; Anode materials

1. Introduction

New lithium storage materials with high gravimetric and volumetric charge capacity and excellent cycle performance have attracted great attention. There have been intense investigations on the Si- or Sn- [1,2] based anode materials to replace commercially used carbonaceous ones due to their high theoretical energy density and suitable electrochemical potential versus Li/Li^+. However, strong volume changes in the structure associated with the charge/discharge process will lead to cracking and crumbling of the electrode materials and poor cycle performance [3]. In order to buffer the volume change of lithium alloy electrodes, various composite structures with nano-dispersed active domains have been proposed and discussed, such as Si/C composite [4], hydrobenzamide-capped tin [5], Si/CNT composite [6], Sn–Cu [7], Sn–Sb [8,9], Sn–Ag [10], Sn–Ni [11], Sn–Ca [12]. For intermetallic compounds, active atoms are, in general, dispersed into a matrix of inactive or less active component which can stabilize the morphology. In fact, amorphous tin-based oxide composite, in which nano-tin domains are uniformly dispersed in oxides, has demonstrated large capacity and excellent rechargeability [13].

Mechanical milling has proven to be a powerful technique to produce alloy powders with a homogeneous structure [14]. In this work, nanosized tin alloys are dispersed in oxides via the reduction of tin oxide by metallic reducing agent under high-energy ball-milling. The microstructure and the electrochemical performance as anode materials for lithium ion batteries are investigated.

2. Experimental

2.1. Material preparation

The ball-milling was carried out in a planetary ball mill (Fritsch P-6 planetary Mono Mill). Powder mixtures of SnO, Al and Co and 15 stainless steel grinding balls in the diameter of 10 mm were placed and sealed in an 80 ml stainless steel grinding bowl in an argon-filled glove box. Milling was performed at a rotation rate of 450 rpm for 5 h. The starting materials were SnO powder (Sinopharm Chemical Reagent, 99.99%), Al powder (Sinopharm Chemical Reagent, 100–200 mesh, 99.99%), Co or Ni powder (Sinopharm Chemical Reagent, 200 mesh, 99.99%) weighted in molar ratio of SnO:Al:Co = 1:0.878:0.333 (SnO:Al:Ni = 1:0.878:0.75). The obtained powders were then collected by sieving in 200 mesh size. As a comparison, Sn/Al_2O_3 composite was synthesized at a rotation rate of 350 rpm for 8 h.

The powders prepared were characterized using Philips 3100E diffractometer with Cu Kα radiation. The morphology and microstructure of ball-milled powders were observed with a transmission electron microscopy (JEOL JEM-2010), a

* Corresponding author. Tel.: +86 21 54747667; fax: +86 21 54741297.
E-mail address: yangj723@sjtu.edu.cn (J. Yang).

0378-7753/$ – see front matter © 2007 Elsevier B.V. All rights reserved.
doi:10.1016/j.jpowsour.2007.06.116

scanning electron microscopy (Hitachi S 2150) and an energy dispersive spectroscopy (Oxford INCAX-sight).

2.2. Cells assembling and electrochemical test

Electrodes were prepared by coating a slurry containing 89 wt.% active material, 5 wt.% acetylene black and 6 wt.% LA132 binder (aqueous emulsion containing a copolymer of acrylamide, AM; lithium methacrylate, LiMAA; acrylonitrile, AN) dispersed in deionized water, or 87:5:8 wt.% for samples using polyvinylidene fluoride (PVDF) binder dissolved in *N*-methyl-2-pyrrolidinone (NMP), on a copper foil and followed by drying under vacuum at 120 °C over 3 h. Electrode disks (Φ1.4 cm) were punched from the foil and weighed. Electrochemical behavior of the test materials was examined via CR2016 coin cells with lithium metal counter electrode, Celgard 2700 membrane separator, and electrolyte of 1 M $LiPF_6$ dissolved in the mixture of ethylene carbonate (EC) and dimethyl carbonate (DMC) (1:1 in weight ratio). The model cells were assembled in an argon-filled glove box containing less than 1 ppm each of oxygen and moisture.

Discharge (Li-insertion) and charge (Li-extraction) measurements of the coin cells were carried out at current densities of 0.13 mA mg^{-1} with voltage cut-off of 1.4 V/0.0 V versus Li^+/Li.

3. Results and discussion

Fig. 1 shows the X-ray diffraction (XRD) patterns of three composite samples. XRD responses of $2\theta = 30.6°$, 32°, 43.9°, 45° due to Sn diffractions can be clearly observed in Fig. 1 (S1). XRD peaks at $2\theta = 28.5°$, 33.7°, 35.7°, 43.2°, etc. in Fig. 1 (S2) are related to Sn_3Co phase. In a similar way, Sn_4Ni_3/Al_2O_3 composite can be obtained by replacing Co by Ni. The diffraction peaks at $2\theta = 30.4°$, 43.3°, 44.6° and others in Fig. 1 (S3) correspond to the responses of Sn_4Ni_3 phase. A detectable peak at $2\theta = 45°$ in the three curves is attributed to the common Al_2O_3 product. No precursor components such as SnO, cobalt and nickel can be observed after ball milling. According to the changes of phase compositions caused by ball-milling, the reactions can be described as following:

$$3SnO + 2Al \rightarrow 3Sn + Al_2O_3 \quad (1)$$

$$3Sn + Co \rightarrow Sn_3Co \quad (2)$$

$$4Sn + 3Ni \rightarrow Sn_4Ni_3 \quad (3)$$

Broad peak width and weak diffraction intensity suggest the low-crystalline and fine granular features of the alloys in the composites. It is estimated from XRD pattern and Scherrer equation that crystal size of Sn_3Co alloy is about 10 nm.

It should be mentioned that Sn/Al_2O_3 composite can be easily prepared by SnO reduction under 350 rpm ball-milling. When rotation speed is increased to 450 rpm, the sample can hardly be collected due to strong conglutination of elastic tin on the bowl wall and ball surface. The formation of tin alloys by addition of inert metal Co or Ni will alleviate (or even prevent) conglutination of elastic tin on the bowl wall. In addition, inert cobalt and nickel to lithium can improve elec-

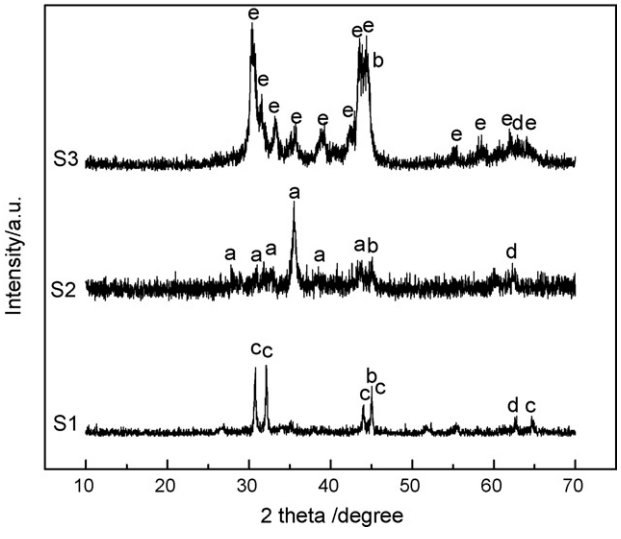

Fig. 1. XRD patterns of (S1) Sn/Al_2O_3 composite, (S2) Sn_3Co/Al_2O_3 composite, (S3) Sn_4Ni_3/Al_2O_3 composite (peak labels: a, Sn_3Co; b, Al_2O_3; c, Sn; d, Al; e, Sn_4Ni_3).

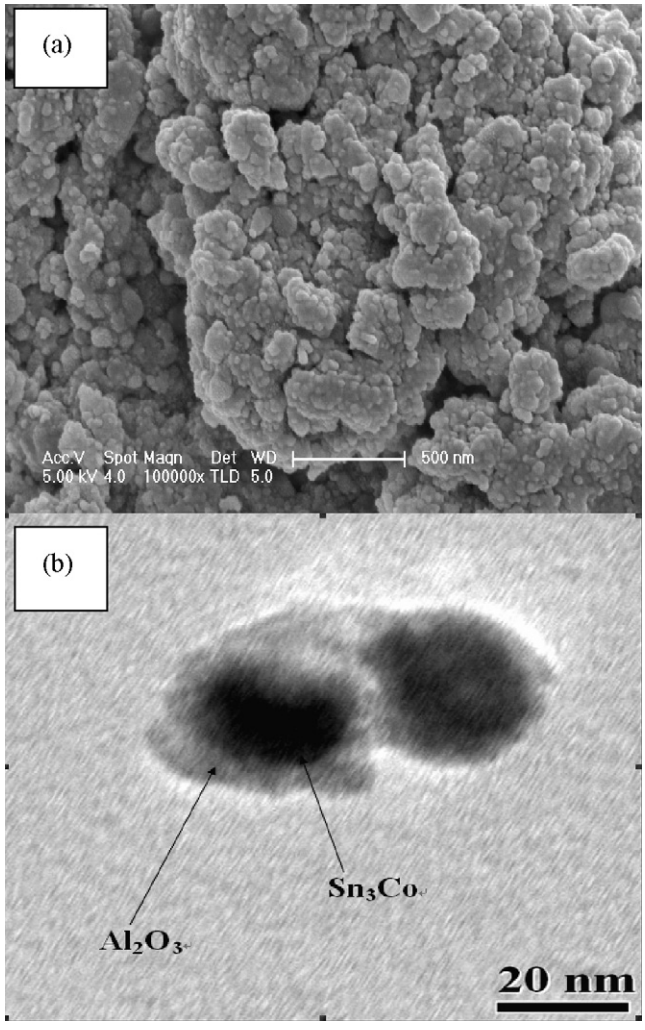

Fig. 2. (a) SEM image of Sn_3Co/Al_2O_3 composite and (b) TEM image of nanosized Sn_3Co/Al_2O_3 composite.

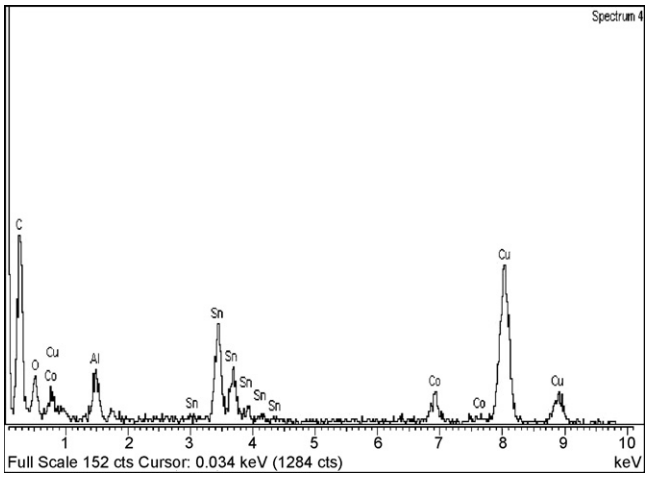

Fig. 3. EDS image of a single particle of nanosized Sn_3Co/Al_2O_3 composite in Fig. 2b.

tronic conductivity of the composites and suppress the volume change.

Fig. 2a presents a SEM picture of the overall morphology of Sn_3Co/Al_2O_3 composite. Irregular particles and their agglomerates can be observed in the scanned area. The morphology of single particles taken by TEM is illustrated in Fig. 2b. The dark part represents Sn_3Co alloy, which is mainly located in the inner region and surrounded by Al_2O_3 layer. It appears that the composite particles possess heterophase structure, in which the Sn_3Co particles with about 20 nm in size are covered by alumina layer in a thickness of several nanometers. The EDS result for a single particle characterized in Fig. 2b is presented in Fig. 3, which confirms the composition of the product. However, it is not clear so far how the small amount of excess Al disperses in the composite. The strong copper and carbon responses are related to the supporting substrate.

Constant current measurements were conducted to characterize the electrochemical performance of the composites. Fig. 4 presents the discharge and charge profiles of Sn_3Co/Al_2O_3 and Sn_4Ni_3/Al_2O_3 composite electrodes with LA132 binder for the 1st, 2nd, 10th, and 35th cycles. The Sn_3Co/Al_2O_3 electrode exhibits the first discharge and charge capacity of 803.2 and 595.9 mA h g^{-1}. The first Li-insertion exhibits a big polarization with the voltage plateau at about 0.25 V versus Li, indicating high resistance for interfacial reaction and slow Li-diffusion kinetics in the composite containing inert and non-conductive Al_2O_3. After electrochemical activation in the first cycle, the voltage plateau is progressively shifted towards higher voltage values in the subsequent cycles.

Comparing (a) with (b) in Fig. 4, it is noted that the first Li-insertion trends are quite different for the two samples. The

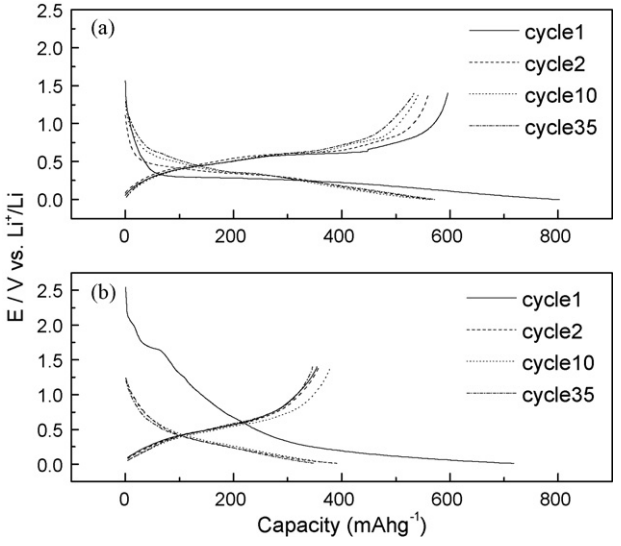

Fig. 4. Discharge and charge profiles of tin-based composite electrodes containing LA132 binder: (a) Sn_3Co/Al_2O_3 and (b) Sn_4Ni_3/Al_2O_3.

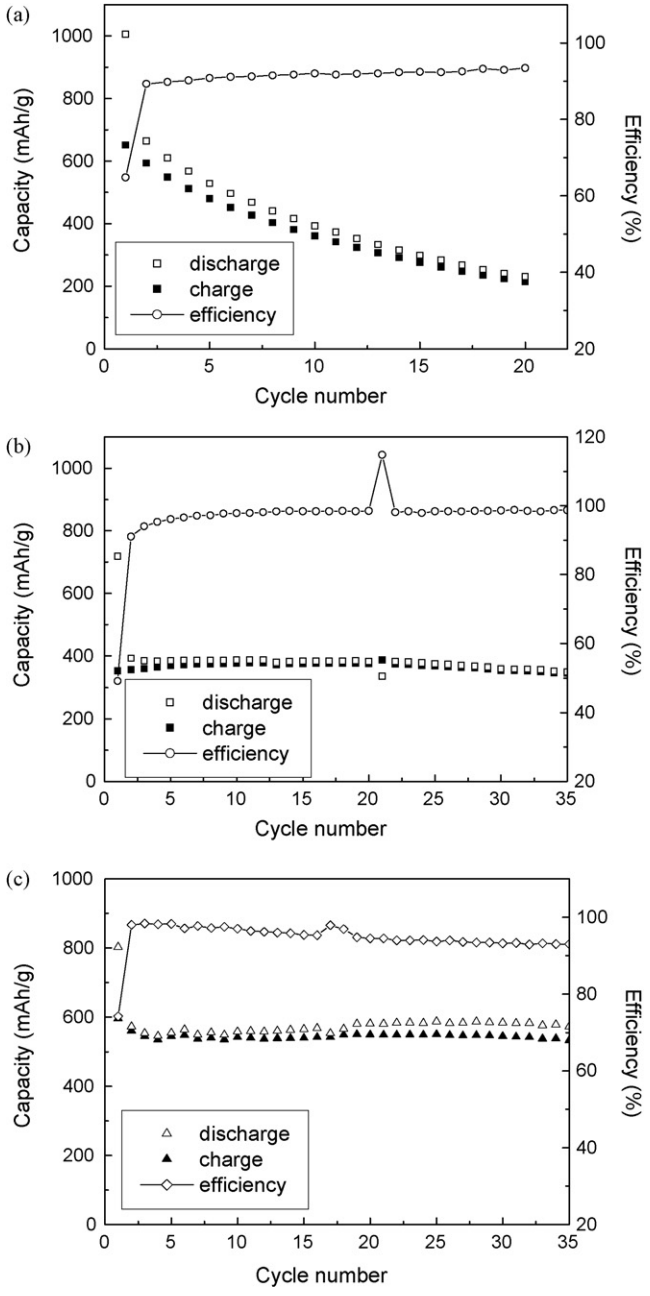

Fig. 5. The cycle performance and efficiency of Sn-based composite electrodes containing LA132 binder: (a) Sn/Al_2O_3; (b) Sn_4Ni_3/Al_2O_3; (c) Sn_3Co/Al_2O_3.

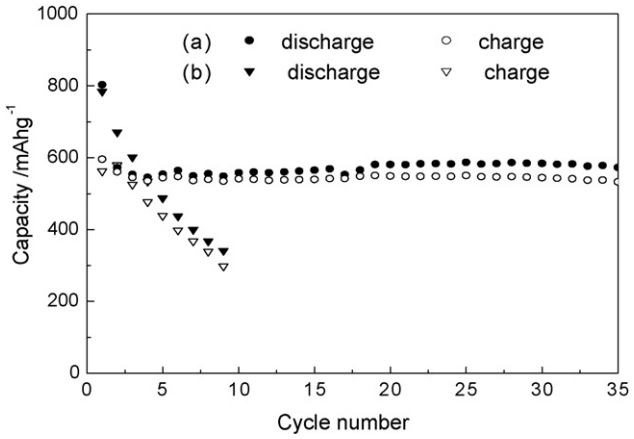

Fig. 6. The cycle performance of Sn_3Co/Al_2O_3 composite electrode containing: (a) LA132 binder and (b) PVDF binder.

capacity in the high voltage range above 0.7 V versus Li for Sn_4Ni_3/Al_2O_3 appears to be related to an irreversible reaction of some active oxide. It is presumed that relatively high Ni content may inhibit a complete reduction of SnO and a small amount of amorphous SnO may remain in the sample. In fact, the initial efficiency is only 49.2% for Sn_4Ni_3/Al_2O_3, much lower than 74.2% of the Sn_3Co/Al_2O_3 electrode. The Sn_4Ni_3/Al_2O_3 electrode exhibits the high initial irreversibility. Moreover, because of the high content of inert nickel, The Sn_4Ni_3/Al_2O_3 electrode presents a low reversible capacity (only ca. 354 mA h g^{-1}).

The cycle capacity and efficiency of Sn/Al_2O_3, Sn_3Co/Al_2O_3 and Sn_4Ni_3/Al_2O_3 electrodes with LA132 binder are given in Fig. 5. Sn/Al_2O_3 composite shows rapid fade in capacity during cycling. The capacity retention is significantly improved by the addition of cobalt. The Sn_3Co/Al_2O_3 electrode shows an overall capacity fade of 0.15% loss per cycle until the 35th cycle. The coulombic efficiency increases from 74.2% in the first cycle to over 94% in the subsequent cycles. During 35 cycles the reversible capacity and efficiency of the Sn_4Ni_3/Al_2O_3 electrode are also stable. The columbic efficiency reaches more than 98% after several cycles. Although in situ formed Al_2O_3 is a good dispersant and buffer matrix, it is insulator and cannot offer electronic conductivity for the active domains. Addition of inert Co or Ni metals improves the electronic conductivity. Moreover, unlike ductile tin which has the tendency to agglomerate under milling, Sn_3Co and Sn_4Ni_3 alloys are relatively brittle and easy to be dispersed. As a result, the tin alloy composite exhibits better cycle stability than Sn/Al_2O_3.

Fig. 6 shows the cycle performance of Sn_3Co/Al_2O_3 composite electrodes containing different types of binders. Binder influence on the electrochemical behavior of electrodes with strong volume change has been investigated by several research groups [15–18]. Concerning the alloy composites in this study, the binder function is critical for the rechargeability. With PVDF binder, the Sn_3Co/Al_2O_3 electrode shows rapid capacity fading. The electrode using LA132 binder, however, exhibits much better cycle stability. This can be explained by the different binding strengths and swelling behavior in the organic electrolyte. Test results show that peeling strength of LA132 binder on a Cu strip in 25 mm width is about 14 times as large as that of PVDF and the swelling of the latter is much more serious.

4. Conclusions

Nanosized tin alloy/Al_2O_3 composites were synthesized by high-energy ball-milling. The combined analysis involving XRD, SEM, TEM, and EDS reveals that Sn_3Co nanoparticles are finely dispersed in the alumina matrix. The results of electrochemical experiments show that the Sn_3Co/Al_2O_3 and Sn_4Ni_3/Al_2O_3 composites as electrode materials have better cycle performance than Sn/Al_2O_3. The Sn_3Co/Al_2O_3 composite electrode containing LA132 binder delivers a stable capacity of ca. 540 mA h g^{-1} which could be maintained over 35 cycles. The improved cycle ability can be contributed to enhanced conductivity of the composite and finer dispersion of active domains. Electrode binder is another important factor influencing the electrode behavior. LA132 binder in aqueous emulsion is fit for the alloy composite electrode owing to its strong binding strength and weak swelling effect in organic electrolytes.

References

[1] Z.H. Chen, V. Chevrier, L. Christensen, J.R. Dahn, Electrochem. Solid-State Lett. 7 (2004) A310.
[2] M. Suzuki, J.J. Suzuki, K. Sekine, T. Takamura, J. Power Sources 146 (2005) 452.
[3] J. Yang, Y. Takeda, N. Imanishi, O. Yamamoto, J. Electrochem. Soc. 146 (1999) 4009.
[4] Z.S. Wen, J. Yang, B.F. Wang, K. Wang, Y. Liu, Electrochem. Commun. 165 (2003) 5.
[5] Y. Kwon, M.G. Kim, Y. Kim, Y. Lee, J. Cho, Electrochem. Solid-State Lett. 9 (2006) A34.
[6] J. Shu, H. Li, R.Z. Yang, Y. Shi, X.J. Huang, Electrochem. Commun. 8 (2005) 51.
[7] J. Wolfenstine, S. Campos, D. Foster, J. Read, W.K. Behl, J. Power Sources 109 (2002) 230.
[8] J. Yang, Y. Takeda, N. Imanishi, T. Ichikawa, O. Yamamoto, Solid State Ionics 135 (2000) 175.
[9] H.L. Zhao, D.H.L. Ng, Z.Q. Lu, N.G. Ma, J. Alloys Compd. 395 (2005) 192.
[10] M. Wachtler, M. Winter, J.O. Besenhard, J. Power Sources 105 (2002) 151.
[11] X.Q. Cheng, P.F. Shi, J. Alloys Compd. 391 (2005) 241.
[12] L. Fang, B.V.R. Chowdari, J. Power Sources 97–98 (2001) 181.
[13] Y. Idota, T. Kubota, A. Matsufuji, Y. Maekawa, T. Miyasaka, Science 276 (1997) 1395.
[14] C.S. Wang, G.T. Wu, X.B. Zhang, Z.F. Qi, W.Z. Li, J. Electrochem. Soc. 145 (1998) 2751.
[15] W.R. Liu, M.H. Yang, H.C. Wu, S.M. Chiao, N.L. Wu, Electrochem. Solid-State Lett. 8 (2005) A100.
[16] N. Dimov, H. Noguchi, M. Yoshio, J. Power Sources 156 (2005) 567.
[17] J.H. Lee, S. Lee, U. Paik, Y.M. Choi, J. Power Sources 147 (2005) 249.
[18] Z. Chen, L. Christensen, J.R. Dahn, J. Electrochem. Soc. 150 (2003) A1073.